JOURNAL OF APPLIED ELECTROCHEMISTRY 8 (1978) 313–326

Dissolution of nickel (74%)-copper (4%)-sulphide matte anode in acidic chloride solutions

D. V. SUBRAHMANYAM, E. L. GHALI

Centre de Recherche du Moyen Nord, Université du Québec à Chicoutimi, Chicoutimi, Québec, Canada

Received 6 September 1977

A comparative study was conducted to assess the performance of 1 N solutions of hydrochloric acid, ferrous chloride and ferric chloride solutions to dissolve the 74% Ni–4% Cu–20% S nickel sulphide matte anodes. The essential variables considered here were: temperature (25° and 75° C), oxygen and controlled potential. The relative aggressiveness as estimated by the potentiokinetic polarization curves and dissolution experiments with open circuit can be arranged in the following sequence:

$$Fe^{3+} > Fe^{2+} > H^{+} .$$

At +400 mV versus SCE, the aggressiveness reversed in the following sequence:

$$H^{+} > Fe^{2+} > Fe^{3+} .$$

The experimental values of dissolution rates with open circuit and at constant potential were higher than those calculated from the dissolution current densities (potentiokinetic polarization curves), and from the amount of charge passed (at +400 mV versus SCE).

Attack by intergranular dissolution and pitting was observed throughout these experiments. The formation of β-NiS by the reaction $Ni_3S_2 \rightarrow Ni^{2+} + 2\beta\text{-NiS} + 2e$ was confirmed by X-ray analysis. The above results are interpreted in the light of the possible electrochemical mechanisms.

1. Introduction

A sulphate–chloride electrolyte, which is well known for the electrodeposition of nickel is also widely used for the electrowinning of nickel and associated metal values from their sulphide-based converter matte anodes [1]. The same electrolyte is also used for the electrorefining of scrap nickel. The usual operating conditions are: initial pH 2, temperature 60° C, and current density 10–40 mA cm^{-2} [1–11]. The presence of chloride as sodium chloride (1 N concentration) maintains the sulphide anode in an active dissolution condition [4–10]. Recently, hydrochloric acid solutions [12, 13] have been tested to dissolve nickel sulphide matte anodes. A flow sheet has been developed for the dissolution of 26% Cu, 48% Ni and 21% S ground mattes in 9 N hydrochloric acid solution [12] at 65° C. To avoid the problem of hydrogen sulphide, acidic metallic chloride solutions belonging to the alkali metal, alkaline earth metal and transition metal groups have also been tested [14–17]. The ferrous and ferric chloride solutions are the most widely tested electrolytes among the transition metal chloride solutions [14–17].

In order to promote the unconventional dissolving agents, i.e., hydrochloric acid, ferrous chloride, and ferric chloride to the conventional utilization level, it is absolutely essential to understand the underlying electrochemistry of the nickel sulphide dissolution. Such an understanding is lacking with respect to the above three electrolyte–nickel sulphide systems. Hence, a systematic study has been conducted in order to rationalize the dissolution and electrochemical behaviour of converter matte anodes containing 74% nickel, 4% copper and 20% sulphur in 1 N solutions of hydrochloric acid, ferrous chloride and ferric chloride. The key parameters considered were: time, temperature, oxygen and applied potential. A substantial attempt was also made to

examine the influence of the above parameters on the morphology of attack and phase change. The above electrode composition is quite significant from the viewpoint of the INCO practices [1].

2. Experimental

The nickel sulphide matte anode supplied by the INCO refinery, Port Colborne, Ontario, had the following composition: 74 wt% Ni, 4 wt% Cu, 0·5 wt% Fe, 0·6 wt% Co, and 20 wt% S. The X-ray diffraction pattern of the polished*–etched† anode revealed (Fig. 13) the presence of Ni_3S_2 (ASTM 8-126), $Cu_{1.96}S$ (ASTM 17-449) and Ni (ASTM 4·0850) phases having hexagonal, ($a_0 = 0{\cdot}574$ nm, $C_0 = 0{\cdot}7139$ nm), tetragonal ($a_0 = 0{\cdot}3996$ nm, $C_0 = 1{\cdot}1287$ nm) and face-centred cubic structures ($a_0 = 0{\cdot}35238$ nm), respectively. The photomicrograph (Fig. 1a) showed the presence of a light grey rounded phase and a nearly square white platelet phase. An electron-microprobe scan (Fig. 1b) indicated the presence of sulphur and copper in the greyish phase, and the presence of nickel and copper in the white platelet, although in small amounts, there is an enrichment of copper at the edges of the nickel precipitate. The nickel phase detected by X-ray analysis can actually be a nickel-rich nickel–copper alloy having its lattice constant very close to that of pure nickel. These observations are in accordance with the thermodynamic phase diagram for the Ni–Cu–S system favouring the formation of Ni_3S_2 (heazlewoodite), $Cu_{1.96}S$ and Cu–Ni alloy phases during the cooling of the converter melts, having the composition mentioned above.

The electrode design is shown in Fig. 2a. The matte anode was machined to a 1 cm diameter disc, soldered to an insulated wire for electrical contact, and then mounted in bakelite after passing through a glass tube. The type of cell that is given in Fig. 2b had provisions for nitrogen gas, water condenser, water circulation, reference, working and counter electrodes, and solution-drain-tap. The luggin probe of the saturated KCl–agar bridge came quite close to the working electrode to avoid *IR*-drops. The electrochemical

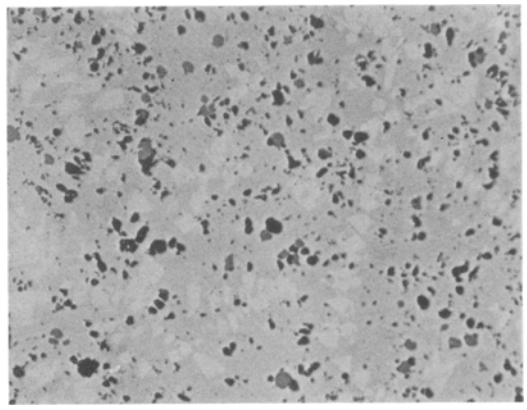

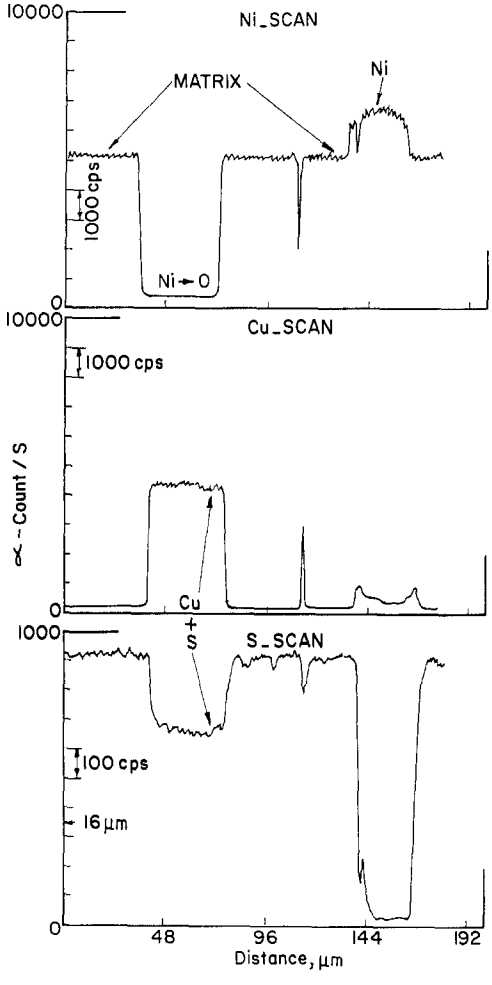

Fig. 1. Photomicrograph and electron microprobe scans of the polished nickel–copper sulphide.
(a) Photomicrograph (× 105).
(b) Electronmicroprobe scans.

* Polished on 240–600 grit wet emery papers, and then, on cloth polishing wheel embedded with 0·05 μm alumina suspension.
† Etched in 1 N HCl for 10 s.

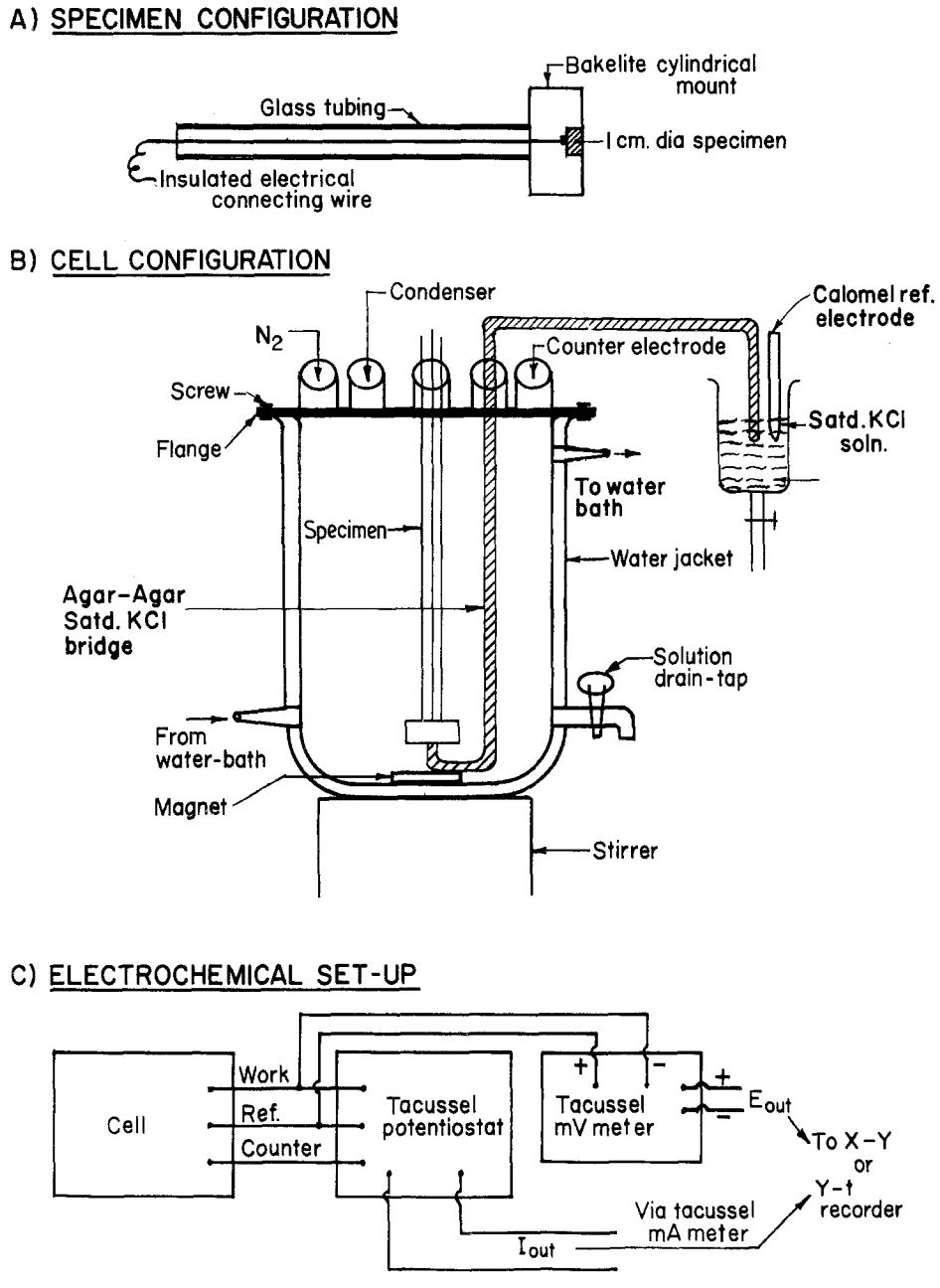

Fig. 2. Experimental arrangement for dissolution and electrochemical measurements.

set-up, shown in Fig. 2c, was conventional in character. A saturated calomel electrode was used as the reference electrode, and all the potentials in this paper are given with respect to this electrode. A graphite rod was used as a counter electrode.

For each experiment, the polished electrode was treated with hydrochloric acid for 1 min, to relieve the strain and dissolve the surface films formed during polishing. Then, it was finally pre-reduced at −600 mV versus SCE in hydrochloric acid solution for 15 min, before making the electrochemical measurements. This value was chosen from the preliminary potentiokinetic polarization curves. The last step was not adopted in ferrous or ferric chloride solutions to prevent

the reduction of ferrous or ferric ions. Each electrode was used twice. Every experiment was duplicated by using one fresh and one used electrode.

The experiments were done with stirred solutions of 1 N HCl, 1 N $FeCl_2$ and 1 N $FeCl_3$. The pH of the latter two solutions was adjusted to pH 0·3 with sulphuric acid solution to keep the chloride concentration constant. For each experiment, 1000 ml of solution was taken. The following was the sequence of experiments:

(a) The potentiokinetic polarization curves of the polished nickel sulphide electrodes (scan rate 500 mV h^{-1}) were obtained in oxygen-free i.e., nitrogen-saturated, and oxygen-saturated solutions at 25° and 75° C.

(b) The amounts of nickel and copper dissolved from the sulphide with open circuit and at constant potential were determined as a function of time by atomic absorption analyses of 8–10 ml samples drawn at regular intervals.

(c) The morphology of attack was determined with a Unitron microscope and the crystal structure with a Phillips X-ray Diffractometer (CuKα radiation).

3. Results

3.1. *Potentiokinetic polarization curves*

The potentiokinetic polarization curves of 74% nickel–4% copper sulphide electrode in stirred 1 N HCl, 1 N $FeCl_2$ and 1 N $FeCl_3$ solutions are shown in Figs. 3–5. In certain instances, the cathodic and anodic curves consisted of linear portions corresponding to the electrochemical, i.e. charge transfer-controlled step, and non-linear portions signifying cathodic and anodic limiting current densities. The limiting current densities can be caused by the two factors: (i) diffusion control at the solution–nickel sulphide interface or in bulk solution itself; (ii) space-charge limited currents caused by electron and or hole transport, provided the nickel–copper sulphide is assumed to behave as a low energy-gap semiconductor. The point of intersection of the linear portions of the polarization curves gives the values of the dissolution potentials and corresponding dissolution current densities. The electrode parameters, i.e., Tafel slopes, dissolution potentials, and critical potentials (potential corresponding to anodic limiting cur-

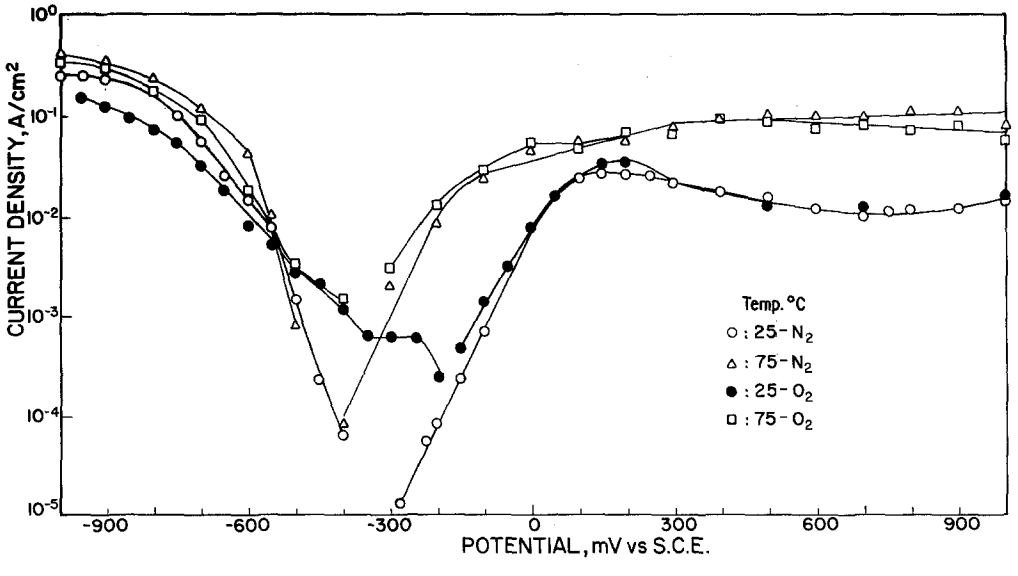

Fig. 3. Potentiokinetic polarization curves of nickel–copper sulphide in stirred 1 N HCl solutions. Scan rate 500 mV h^{-1} in all cases.

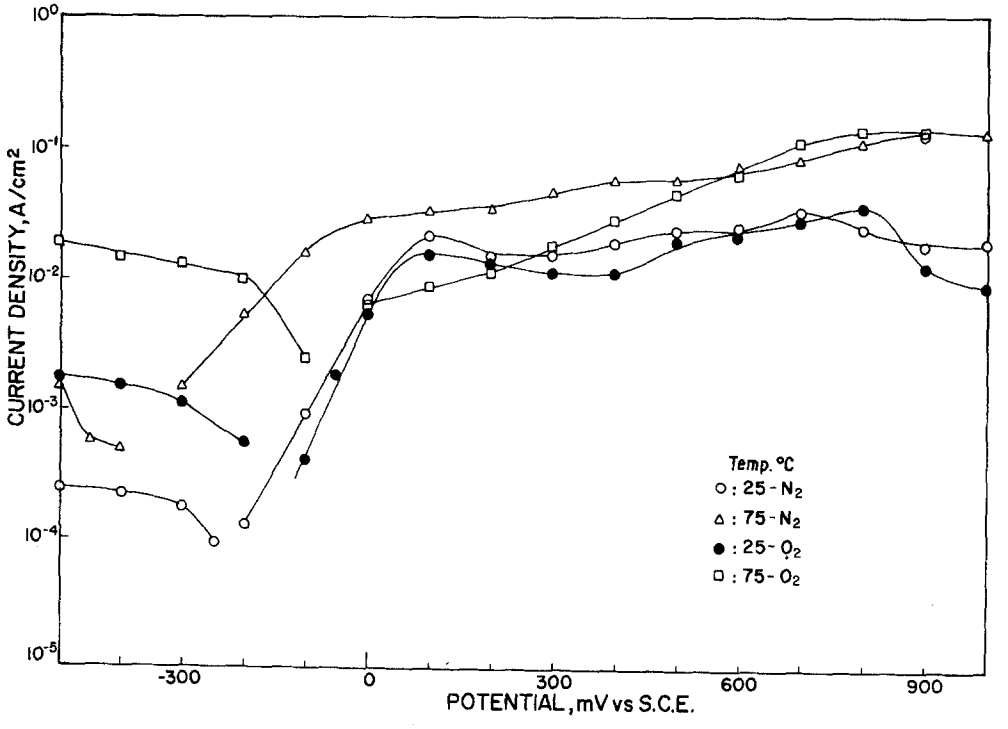

Fig. 4. Potentiokinetic polarization curves of nickel–copper sulphide in stirred 1 N $FeCl_2$ solutions.

Table 1. Electrode parameters of nickel–copper–sulphide in hydrochloric acid, ferrous chloride and ferric chloride solutions using stirred solutions (Concentration 1 N; pH 0·1–0·3). Values obtained from the polarization curves in Figs. 3–5

Condition	*Tafel slopes* (mV decade^{-1})		*Potential* (mV versus SCE)		*Current density* (mA cm^{-2})	
	Cathodic	*Anodic*	*Dissolution*	*Critical*	*Dissolution*	*Critical*
1. HCl						
(a) 25° C – N_2	–75	+105	–325	+100	0·006	28
(b) 25° C – O_2	very high	+120	–220	+150	0·160	32
(c) 75° C – N_2	–60	+100	–430	–100	0·048	50
(d) 75° C – O_2		very high	–420	–100	0·650	60
2. $FeCl_2$						
(a) 25° C – N_2	very high	+115	–200	+100	0·130	17
(b) 25° C – O_2	very high	+100	–100	+100	0·450	16
(c) 75° C – N_2	very high	very high	–400	0	0·500	28
(d) 75° C – O_2	very high	very high	–130	?*	4·500	?*
3. $FeCl_3$						
(a) 25° C – N_2	very high	very high	+400	+500	2·90	6
(b) 25° C – O_2	very high	very high	+450	+450	5·00	8
(c) 75° C – N_2	very high	very high	+350	+500	5·60	34
(d) 75° C – O_2	very high	very high	+315	+500	5·60	38

* Critical potential cannot be determined with satisfactory precision.

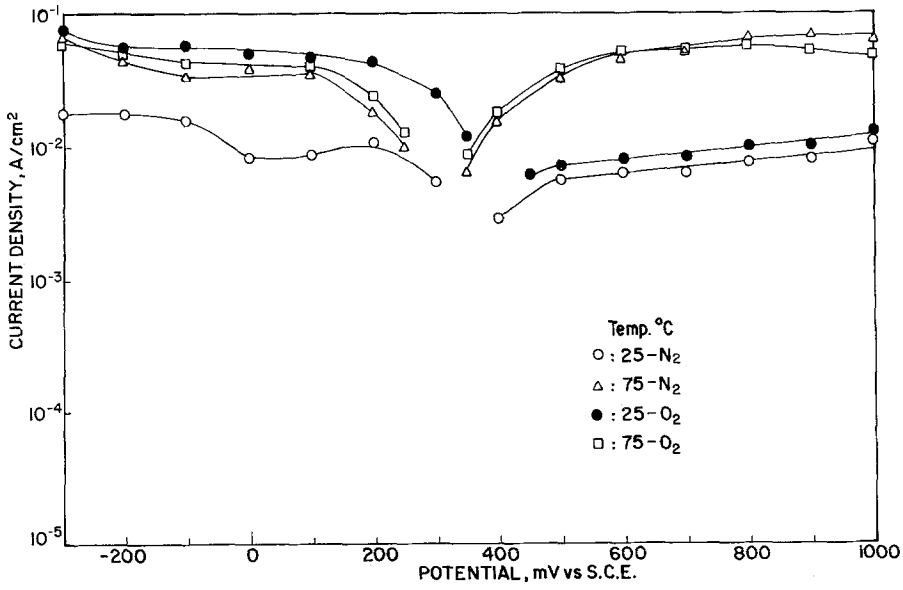

Fig. 5. Potentiokinetic polarization curves of nickel–copper sulphide in stirred 1 N $FeCl_3$ solutions.

rent density), and the dissolution and anodic limiting current densities are given in Table 1.

In hydrochloric acid solutions free of oxygen (nitrogen-saturated solutions), nickel–copper sulphide exhibits Tafel behaviour (Fig. 3, Table 1). The cathodic and anodic Tafel slopes are −75 mV decade^{-1} and +105 mV decade^{-1}, respectively. At 75° C, these slopes do not vary significantly. The presence of oxygen results in higher Tafel slopes, indicating that the dissolution is under mixed control of charge-transfer and mass-transfer (diffusion). The rest potential (−325 mV) as well as the critical potential (+100 mV) at 25° C becomes more active at 75° C, and more noble with oxygen at 25° C. These potentials are not influenced by oxygen at 75° C. The cathodic curves showed an early depolarization and subsequent overpolarization by oxygen. The overpolarization may be due to slow product removal from the electrode surface. The anodic part is unaffected by oxygen. The dissolution and critical current densities are increased by an increase in temperature. Oxygen seems to be more effective at 25° C than at 75° C. At a later stage in this paper, the rates estimated from the polarization curves will be compared with the measured dissolution rates of copper–nickel sulphide in hydrochloric acid, ferrous, and ferric chloride solutions.

In ferrous chloride solutions, the anodic Tafel slopes in oxygen-free and oxygen-containing solutions are more or less the same as those in the hydrochloric acid solutions (Table 1). The high Tafel slopes and flat polarization curves under other conditions signify the diffusion-controlled dissolution. Cathodic polarization curves exhibit relatively larger depolarization in presence of oxygen (Fig. 4) than the anodic branch. At 75° C, the anodic polarization curves exhibit initial depolarization up to +500 mV. The temperature and oxygen changed the potentials and current densities in the same direction as in the hydrochloric acid solutions. The flat polarization curves in ferric chloride solutions lead to conclusions similar to those for ferrous chloride solutions (Fig. 5). The influence of oxygen on the cathodic and anodic polarization curves is less significant when compared to those in ferrous chloride solutions. The potentials and current densities are at a maximum in ferric chloride solutions. Based on the dissolution current densities (Table 1), the relative aggressiveness with open circuit can be arranged in the following sequence:

$$Fe^{3+} > Fe^{2+} > H^+ .$$

Throughout these experiments, the chloride ion concentration was kept constant. It is assumed that the sulphate ion addition, as sulphuric acid, to keep the pH constant does not have significant effect on the above conclusions.

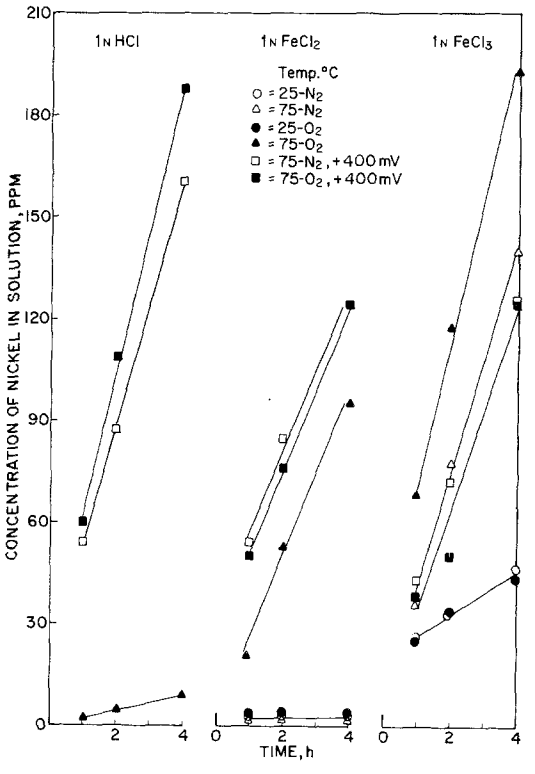

Fig. 6. Dissolution of nickel from nickel–copper sulphide versus time curves in stirred solutions of 1 N HCl, 1 N $FeCl_2$ and 1 N $FeCl_3$.

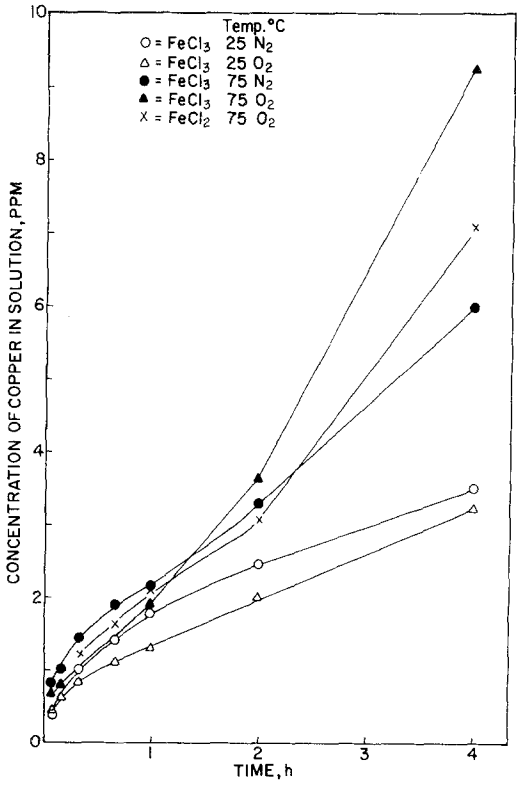

Fig. 7. Dissolution of copper from nickel–copper sulphide versus time curves in stirred solutions of 1 N $FeCl_2$ and 1 N $FeCl_3$.

3.2. *Dissolution rates*

The changes in nickel and copper concentration in the solution with time, i.e., concentration ($g\ l^{-1}$)–time curves (Figs. 6 and 7) are related to the dissolution rates of the nickel copper sulphide (74% Ni–4% Cu–20% S). The relative positions of these curves determine the solution aggressiveness (HCl versus $FeCl_2$ versus $FeCl_3$) as a function of dissolved oxygen, temperature and applied potential (+400 mV). The dissolution of iron (0·5%) and cobalt (0·6%) from the sulphide was not followed due to their presence in the solution in only trace amounts (beyond analytical limits). Further, the changes in copper concentration in the solution with time at constant potential (+400 mV) were excluded because part of the dissolved copper was plating out on the graphite counterelectrode.

In hydrochloric acid solutions, at 25° C, the amounts of nickel and copper formed were extremely low, thus corresponding to the low dissolution rates of sulphides (Figs. 6 and 7). At 75° C, the addition of oxygen to saturation increased the rates with open circuit, as well as at an applied potential of +400 mV. In the 1 N ferrous chloride and ferric chloride solutions, the rates were not increased significantly by oxygen at 25° C. The relative increase in rate by oxygen was highest in ferrous chloride solutions. At constant potential, the presence of oxygen did not change the dissolution rates significantly. An oxygenated ferric chloride solution was the most aggressive medium to dissolve the sulphide with open circuit, whereas oxygenated hydrochloric acid solution was most aggressive at +400 mV. The following sequence of aggressiveness can be set up with open circuit and at constant potential:

Table 2. Nickel and copper build-up rates with time (from Figs. 6 and 7) using 1 N stirred solutions

Solution and conditions	*Nickel build-up rate* ($mg\,h^{-1}\,cm^{-2}$)			*Copper build-up rate* ($mg\,h^{-1}\,cm^{-2}$)		
	1 min	*1 h*	*4 h*	*1 min*	*1 h*	*4 h*
HCl						
75° C – O_2	–	2·5	2·5	–	–	–
75° C – N_2 +400 mV	343·0	56·0	40·0	–	–	–
75° C – O_2 +400 mV	445·0	76·0	60·0	–	–	–
$FeCl_2$						
25° C – N_2, O_2	–	3·1	0·8	– negligible		
75° C – N_2	–	23·0	30·2	–	2·8	2·3
75° C – N_2 +400 mV	458·0	69·0	39·0	–	–	–
75° C – O_2 +400 mV	374·0	64·0	39·4	–	–	–
$FeCl_3$						
25° C – N_2	191·0	34·3	15·0	23·0	2·3	1·1
25° C – O_2	229·0	32·0	14·0	27·0	1·7	1·0
75° C – N_2	333·0	52·0	45·0	32·0	2·7	1·4
75° C – O_2	336·0	85·2	61·3	29·0	2·4	2·9
75° C – N_2 +400 mV	347·0	55·0	40·1	–	–	–
75° C – O_2 +400 mV	260	37·0	39·4	–	–	–

open circuit: $Fe^{3+}(O_2) > Fe^{2+}(O_2) > H^+(O_2)$

constant potential: $H^+ > Fe^{2+}(O_2, N_2) > Fe^{3+}(O_2, N_2)$.

The observed aggressiveness pattern on open-circuit dissolution is the same as that predicted from potentiokinetic polarization curves. From Figs. 6 and 7, the instantaneous nickel and copper build up rates in 1 N solutions of hydrochloric acid, ferrous chloride and ferric chloride are calculated at 1 min, 1 h and 4 h intervals and given in Table 2. In general, the nickel and copper build-up rates decreased with time, corresponding to the decreasing sulphide dissolution rates with time. A reverse effect was observed for the open circuit dissolution in oxygen-saturated ferrous chloride solutions at 75° C.

To account for the sharp increase in rates in oxygenated ferrous chloride solutions at 75° C, the ferric ion was titrated (10 ml sample) against a standard solution of the disodium salt of ethylene diammine tetraacetic acid using sulphosalicylic acid as indicator. Fig. 8 shows that the formation of ferric ion was quite rapid in oxygen-saturated solutions in comparison to that in the nitrogen-saturated (oxygen-free) solutions. At constant potential, there was a slight retardation of the formation of ferric ion in oxygenated solution. Thus, in the presence of oxygen, 2·2 g l^{-1} of ferric

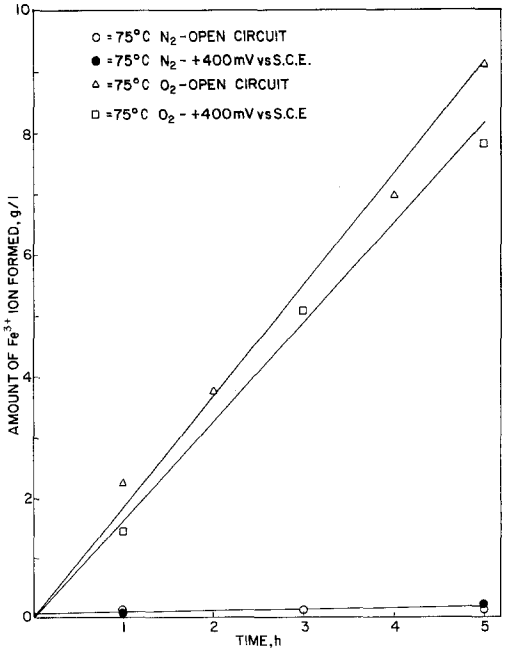

Fig. 8. Build-up of Fe^{3+} in 1 N $FeCl_2$ solutions with time.

ion was formed during the one hour thermostating and this was sufficient to enhance the dissolution rate of sulphide. With time, the rate increases further, as the amount of ferric ion in solution increases to a final value of 9 g l^{-1}.

The phenomenon of preferential dissolution can be viewed by comparing the nickel to nickel plus copper percentages in the solid to those in solution (Table 2, Fig. 9). The percentage of nickel–nickel plus copper in the solid is 95%. During the one minute interval, the nickel percentages in solution (80–90%) corresponded to the preferential dissolution of copper from the $Cu_{1.96}S$ and Ni–Cu alloy phases in ferrous and ferric chloride solutions. At higher durations, the nickel percentage in solution is almost the same as that in the solid, thus suggesting that the preferential dissolution of copper from its corresponding phases is negligible.

3.3. *Potential–time and current–time curves*

The potential–time curves of the sulphide electrode immersed in 1 N solutions of hydrochloric acid, ferrous chloride and ferric chloride are shown in Fig. 10. The features which are quite common in this figure are that the potential becomes more active with an increase of temperature, and more noble with the oxygen-saturated solutions. The potential difference between the oxygen- and nitrogen-saturated solution was a maximum (500 mV) with a ferrous chloride medium. In the same way, the maximum positive difference in potential occurred in the oxygen-saturated ferrous chloride solution (final potential − initial potential = 550 mV). A noble shift in potential is due to the formation of ferric ion (see Fig. 8). In ferric chloride solutions, too, the potential increased sharply during the first hour and then became more or less steady. The potential changes with time were insignificant in hydrochloric acid solutions. In the case of hydrochloric acid solutions, the dissolution potentials obtained from potential–time curves (Fig. 10) and the potentials determined from potentiokinetic polarization curves are in excellent agreement. The lack of agreement in ferrous and ferric

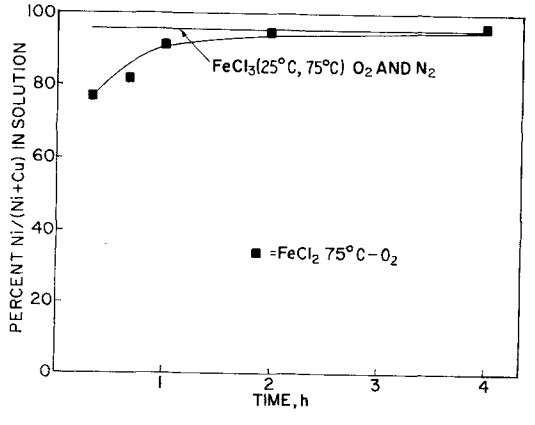

Fig. 9. Change in percentage of Ni/Ni + Cu in solution with time.

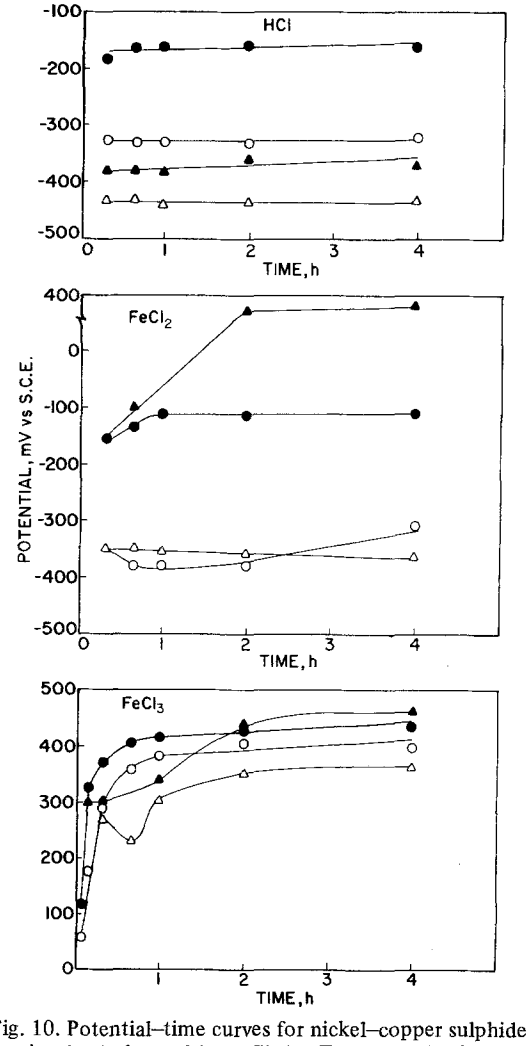

Fig. 10. Potential–time curves for nickel–copper sulphide in stirred solutions of 1 N HCl, 1 N $FeCl_2$ and 1 N $FeCl_3$.
○ 25°–N_2
● 25°–O_2
△ 75°–N_2
▲ 75°–O_2 .

chloride solutions may be due to the fact that longer durations were required for the dissolution potentials to reach a steady-state value.

The current–time curves of the sulphide electrode dissolving at an anodic potential of +400 mV versus SCE in 1 N HCl, 1 N $FeCl_2$, and 1 N $FeCl_3$ solutions at 75° C with and without oxygen are shown in Fig. 11. At this potential the anodic currents, which were decreasing with time, were maximum (i_{intial} = 260 mA, i_{final} = 56 mA) in hydrochloric acid solutions. The minimum transient occurred in ferric chloride solutions. The currents shifted to cathodic values in ferric chloride solutions after 2 h due to the applied potential being close to the dissolution potential with open circuit (425–450 mV, see Fig. 10). The current–time curves for sulphides in nitrogen-saturated hydrochloric acid and ferrous chloride solutions lie between the current–time curves for sulphide in oxygenated hydrochloric acid solutions and ferric chloride solutions. A decaying anodic transient signifies a rapid decline of the rates with time, as observed in Table 2.

3.4. *Morphology and crystal structure changes*

The photomicrographs of nickel–copper sulphide after its 4 h immersion in 1 N HCl, 1 N $FeCl_2$, and 1 N $FeCl_3$ solutions either with open circuit or at constant potential revealed the following unique pattern with respect to the attacked specimens:

(a) severe grain-boundary dissolution;

(b) pitting;

(c) dissolution of $Cu_{1.96}S$ and Ni–Cu alloy (bluish-grey rounded phase and white platelets in Fig. 1a); and

(d) relatively less intense attack on the matrix.

The above features are illustrated by a typical photomicrograph (Fig. 12).

A typical X-ray diffraction pattern (Fig. 13) of the sulphide exposed to oxygenated ferric chloride solution at 75° C for two hours showed the formation of the β-NiS (millerite) phase. The formation of β-NiS is due to the dissolution of nickel from the Ni_3S_2 (heazlewoodite) phase and consequent change in nickel-to-sulphur ratio from 3:2 to 1:1. The disappearance of the $Cu_{1.96}S$ and Ni–Cu alloy lines correlate with the observations in the photomicrograph. The formation of β-NiS as an intermediate is in accordance with the observations of Umetsu and Kurihara [9] and Sinev [18] during the leaching of sulphide in sulphate, chloride and hydrochloric acid solutions, and the observations while leaching nickel concentrates in ferrous chloride solutions [17].

4. Discussion

4.1. *Potentiokinetic polarization curves*

When a nickel–copper sulphide containing Ni_3S_2, $Cu_{1.96}S$ (approximately Cu_2S) and Ni–Cu alloy (Figs. 1a, 1b and 12) is subjected to cathodic and anodic polarization, the following cathodic and anodic reactions are expected to occur in hydro-

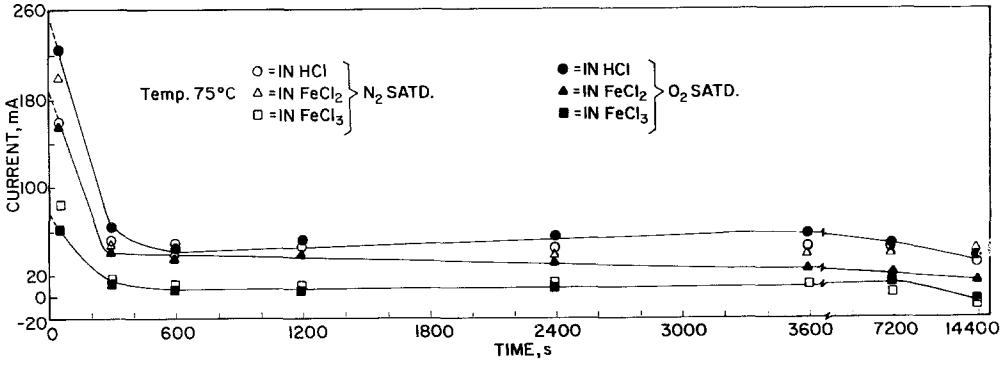

Fig. 11. Current–time curves for nickel–copper sulphide in stirred solutions of 1 N HCl, 1 N $FeCl_2$ and 1 N $FeCl_3$. Potential = +400 mV versus SCE.

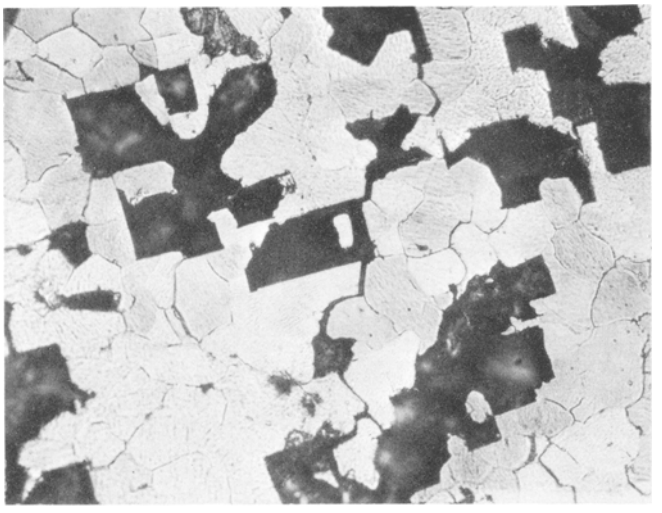

Fig. 12. Photomicrograph of attacked sulphide. $FeCl_3$ 1 N, 75° C, 2 h (× 188).

chloric acid, ferrous chloride (when it contains ferric ion) and ferric chloride solutions:

Cathodic reactions

$$Ni_3S_2 + 6H^+ + 6e \longrightarrow 3Ni + 2H_2S + H_2 \quad \text{(no oxygen)} \quad (1)$$

$$O_2 + 4H^+ + 4e \longrightarrow 2H_2O \; E^0_{25} = +1{\cdot}253 \quad \text{(oxygen present)} \quad (2)$$

$$Fe^{3+} + e \longrightarrow Fe^{2+} \quad (Fe^{3+} \text{ ion present}) \quad (3)$$

Anodic reactions

$$Ni_3S_2 \longrightarrow Ni^{2+} + 2\beta\text{-NiS} + 2e \quad E^0_{25} = +253\ mV_H \quad (4)$$

$$\beta\text{-NiS} \longrightarrow Ni^{2+} + S^0 + 2e \quad E^0_{25} = -197\ mV_H \quad (5)$$

$$S^0 + 4H_2O \longrightarrow SO_4^{2-} + 8H^+ + 6e \quad E^0_{25} = -357\ mV_H \quad (6)$$

$$\text{Ni–Cu alloy} \longrightarrow Ni^{2+} + Cu^{2+} + xe \quad E^0_{25} = +250\ mV_H \quad (7)$$

$$Cu_2S \longrightarrow Cu^{2+} + S^0 + 4e \quad E^0_{25} = -560\ mV_H \quad (8)$$

$$Fe^{2+}, O_2, \text{temp.} \longrightarrow Fe^{3+} + e \quad E^0_{25} = -770\ mV_H. \quad (9)$$

The standard electrode potentials for Reactions 2, 3, 6, 8 and 9 are taken from the literature [19–21]. The standard electrode potentials for the other reactions are calculated on the basis of the values for free energy of formation of Ni_3S_2 [22] (−41·0 kcal mol^{-1}), and β-NiS [23] (−20·5 kcal mol^{-1}) reported in the literature. In the oxygen-free hydrochloric acid solutions, the observed cathodic Tafel slopes of −75 mV (25° C) and −60 mV (75° C) may probably fit into the three-electron transfer reaction of total hydrogen sulphide (and hydrogen) evolution reaction given by Equation 1. When $\alpha = 0{\cdot}5$, this Tafel slope will be $(2 \times 2{\cdot}303\ RT)/(0{\cdot}5 \times nF)$ ($n = 3$) or 40 mV $decade^{-1}$. The observed cathodic Tafel slope is higher than the expected value. Likewise, the anodic Tafel slope of 112 mV $decade^{-1}$ in hydrochloric acid and ferrous chloride solutions is quite high. It is not unusual to observe high cathodic and anodic Tafel slopes with the semi-conducting nickel sulphide since such a response is quite characteristic of the semi-conducting electrode reactions. Possible contributing factors to this type of behaviour are: (i) diffusion control at the sulphide–solution interface or in the bulk electrolyte when oxygen and ferric ions are present, and (ii) impurities on the electrode surface (probably adsorbed).

4.2. *Dissolution rates*

It is demonstrated by the present investigation that

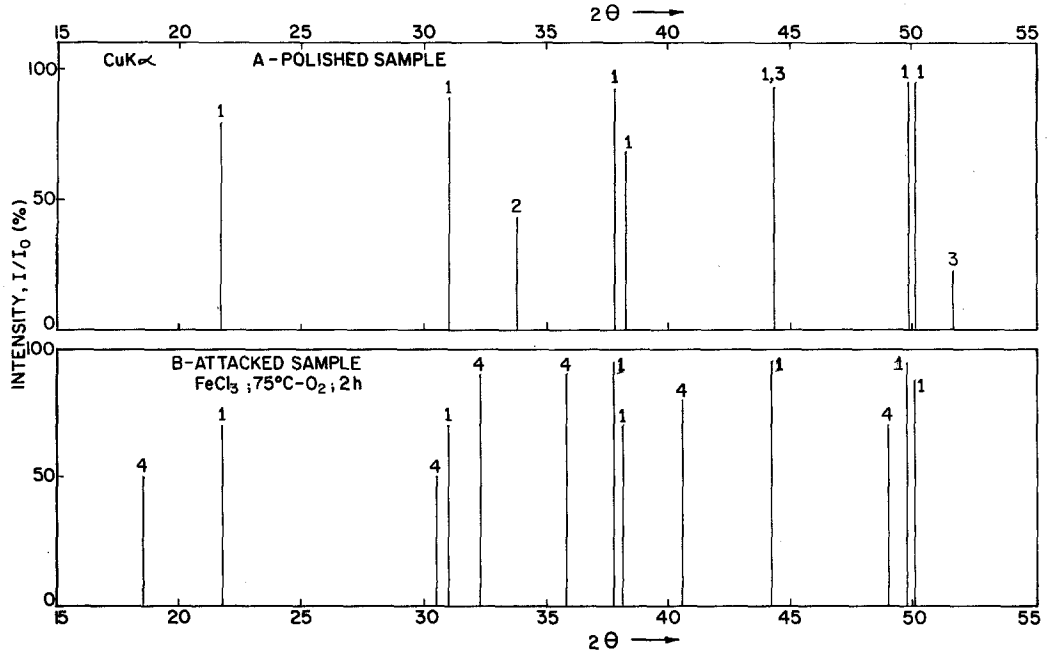

Fig. 13. The X-ray diffraction patterns of polished attacked nickel–copper sulphide.
1. Ni_3S_2;
2. $Cu_{1.96}S$;
3. Ni (probably high Ni–Cu alloy);
4. β-NiS.

an oxygenated ferric chloride solution was most aggressive for the dissolution of the sulphide with open circuit. On the other hand, at constant potential, an oxygenated hydrochloric acid solution was most aggressive with the presence of oxygen lowering the rates in ferrous and ferric chloride solutions. This may be due to the oxygen and ferric ion synergistically causing partial passivity by the formation of oxide films. This supposition needs further experimental support.

Table 3. Comparison between the nickel dissolution rates calculated from the potentiokinetic data and those observed using stirred 1 N solutions

Solution and condition	i_{diss} *from PKPC** (mA cm^{-2})	*Expected rate* (mg cm^{-2} h^{-1})	*Observed rate* (mg $cm^{-2}h^{-1}$)
HCl			
(a) 25° C (O_2, N_2) and 75° C (N_2)	0·006–0·068	0·006–0·71	beyond analysis
(b) 75° C (O_2)	0·65	0·68	2·5
$FeCl_2$			
(a) 25° C (N_2, O_2)	0·13, 0·45	0·14, 0·47	beyond analysis
(b) 75° C – N_2	0·50	0·52	3·1
(c) 75° C – O_2	4·50	4·68	23·0
$FeCl_3$			
(a) 25° C – N_2	2·90	3·1	34·3
(b) 25° C – O_2	5·00	5·2	32·0
(c) 75° C – N_2	5·60	5·8	52·0
(d) 75° C – O_2	5·60	5·8	85·2

* Potentiokinetic polarization curves

Sinev *et al.* [18], during their dissolution studies with the heazelwoodite (Ni_3S_2) phase in hydrochloric acid solutions, have conclusively pointed out that the decline in dissolution rates was associated with the formation of β-NiS. A similar explanation will account for the decrease in rates (with open circuit as well as at constant potential) because of the formation of β-NiS.

The chemical dissolution of sulphide by ferric ion and oxygen was proved by (a) comparing the nickel dissolution rates (mg cm^{-2} h^{-1}) with open circuit to those calculated from the dissolution current densities (Table 1, Figs. 3–5); and (b) by integrating the current–time curves (Fig. 11) and comparing the charge–nickel concentration curves with the calculated curves (Fig. 14). In both cases the following approximations were made:

(a) dissolution of nickel by the overall reaction

$$Ni_3S_2 \rightarrow 3Ni^{2+} + 2S^0 + 6e, \text{ and}$$

$$(Ni\text{–}Cu) \rightarrow Ni^{2+} + 2e, \text{ proceed at the same rate;}$$

and

(b) 95% of each coulomb passed goes to dissolve the combined Ni_3S_2 and Ni phases (1 C ≡ 0·304 mg of Ni^{2+}).

Since the rate in Fig. 9 indicates a negligible initial preferential dissolution of copper, the second assumption is a reasonable one. Such assumptions have to be made in the absence of information on sulphide–sulphur oxidation kinetics. Table 3 shows that the measured open circuit dissolution rates were higher by a factor of at least 10. So also, in Fig. 14, the experimental concentration–charge curves are above the calculated curves. These two features clearly confirm the chemical dissolution by ferric ion. Detailed experiments with pure sulphide phases are needed to separate the electrochemical and non-electrochemical kinetic steps involved during the sulphide dissolution in Fe^{3+} ion-containing solutions.

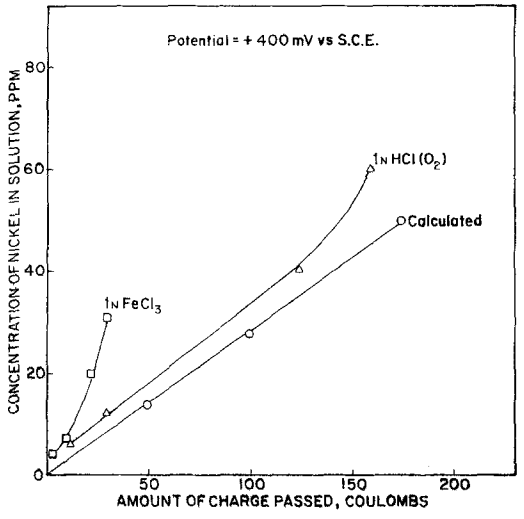

Fig. 14. Quantity of current–nickel concentration curves. Potential = +400 mV versus SCE.

4.3. *Dissolution potentials*

The measured dissolution potentials as functions of the solution type (HCl, $FeCl_2$, and $FeCl_3$), oxygen, temperature and time were in the range −188 mV_H (HCl–N_2 at 75° C)–218 mV_H. The standard potentials for Reactions 1–9 at 75° C are bound to be different from those given above for 25° C, due to the variations in the standard entropies and partial molal heat capacities of the ions. However, the changes in standard potential due to increases in temperature cannot possibly alter the potential limits of the reactions. Thus, in the above interval of potentials, Ni^{2+} ions, Cu^{2+} ions and β-NiS are expected to be the stable species. The potential-determining reactions with the Ni_3S_2 phase are as follows:

(a) HCl solutions without oxygen:

$$Ni_3S_2 + 2H^+ \rightarrow 2\beta\text{-NiS} + Ni^{2+} + H_2 \quad (10)$$

(b) Solutions containing oxygen:

$$Ni_3S_2 + 1/2O_2 + H_2O \rightarrow 2\beta\text{-NiS} + Ni^{2+} + 2OH^- \quad (11)$$

(c) Solutions containing ferric ion:

$$Ni_3S_2 + 2Fe^{3+} \rightarrow 2\beta\text{-NiS} + Ni^{2+} + 2Fe^{2+}. \quad (12)$$

The standard potentials for these reactions vary between 253—1000 mV_H at 25° C. Similar reactions can also be established for the Ni–Cu alloy and $Cu_{1.96}S$ phases.

4.4. *Significance of the results*

If it is possible to develop exotic materials of construction to handle the potentially corrosive leaching media, the hydrochloric acid and ferric chloride solutions offer themselves as suitable choices for leaching and/or electrooxidation of the nickel sulphide converter matte anode. For

instances where pure nickel production is of primary concern, oxygenated hydrochloric acid solutions at controlled electrochemical conditions, i.e., current corresponding to a potential where substantial anodic slimes, which lower the rates, are not produced, are suitable. On the other hand, if the production of ferronickel is the primary concern, then ferrous–ferric chloride mixtures or ferric chloride solutions with open circuit are suitable choices. Otherwise, an elimination of iron from the solution by precipitation and liquid solid separation is quite tedious.

Conclusions

The following conclusions were reached:
(a) Oxygenated ferric chloride and hydrochloric acid solutions were found suitable to dissolve the nickel–copper sulphide matte anode with open circuit and constant potential, respectively.
(b) In the case of ferrous chloride solutions, in the presence of oxygen, the acceleration of the dissolution rate can be attributed to the formation of ferric ion.
(c) The potentiokinetic curves, metal dissolution–time curves and current–time curves signify the existence of diffusion-controlled reactions during the dissolution of sulphide in these media.
(d) The photomicrographs are suggestive of grain-boundary attack, pitting attack and selective attack on the $Cu_{1.96}$ and Ni–Cu alloy phases, and a less severe attack on the Ni_3S_2 phase.
(e) The X-ray diffraction pattern detected the presence of NiS formed by the partial reaction: $Ni_3S_2 \rightarrow Ni^{2+} + 2\beta\text{-NiS} + 2e$.

Acknowledgements

The authors wish to thank Y. Laliberté, G. Castonguay and A. E. Torma for discussions, encouragement and laboratory facilities, F. Claisse (Laval University) for microprobe analysis, and J. Legault (MSc student in our group) for the experimental assistance.

References

[1] J. R. Boldt, 'The Winning of Nickel', Longmans, Canada (1967) p. 270.
[2] M. Loshkarev, O. Esin and G. Lapp, *Zhur. priklad. Khim.* **18** (1945) 294; *Chem. Abs.* **40** (1946) 3343.
[3] L. S. Renzoni, R. C. McQuire and W. V. Barker, *Canad. Chem. Processing* **42** (1958) 72.
[4] *Idem, J. Metals* **10** (1958) 414.
[5] L. S. Renzoni and W. V. Barker, US Patent No. 2 839 461 (1958).
[6] W. W. Spence and W. R. Cook, *Canad. Min. Met. Bull.* **57** (1964) 1181.
[7] D. M. Chizhikov and B. Z. Ustinskii, *Zhur. Priklad. Khim.* **29** (1956) 1129; *Chem. Abs.* **50** (1956) 16 474.
[8] A. A. Bulakh and O. A. Khan, *ibid* **27** (1954) 166; *Chem. Abs.* **48** (1954) 8087.
[9] Y. Umetsu and J. Kurihara, *Nippon Kogyo Kaishi* 78 (1962) 333; *Chem. Abs.* **57** (1963) 8339.
[10] D. M. Chizhikov, 'Issled. Protessov. Tsvet. Redk. Metal' (1969) 159.
[11] D. M. Chizhikov, L. V. Pliginskaya, E. A. Subbotina, N. V. Skorduli and R. I. Komarova, *Electrokhimiya* **9** (1973) 449.
[12] P. G. Thornhill, E. Wigstol and G. Van Weert, *J. Metals* **23** (1971) 13.
[13] N. F. Dyson and T. R. Scott, *Hydrometallurgy* **1** (1976) 361.
[14] P. R. Kruesi, US Patents Nos. 3 736 238 and 3 766 026 (1973).
[15] P. R. Kruesi, E. S. Allen and J. L. Lake, *CIM Bulletin* **6** (1973) 81.
[16] I. J. Corran and M. T. Scholtz, *J. S. African Inst. Mining Metall.* **76** (1976) 403.
[17] E. L. Ghali, B. Girard and D. V. Subrahmanyam, *J. Appl. Electrochem.* **7** (1977) 485.
[18] L. A. Sinev, T. R. Soboleva and E. A. Shamro, *Izv. Vyssh. Uchebn. Zaved. Tsvetn. Metall.* **4** (1975) 35; *Chem. Abs.* **84** (1976) 77300.
[19] M. Pourbaix, 'Atlas of Electrochemical Equilibrias in Aqueous Solutions', NACE, Houston (1966).
[20] O. Kubaschewski, E. El. Evans and C. B. Alcock, 'Metallurgical Thermochemistry', Pergamon Press, London (1967).
[21] R. M. Garrels and C. L. Christ, 'Solutions, Minerals and Equilibria', Harpar and Row (1965).
[22] M. Nagamori and R. T. Ingraham, *Metall. Trans.* **1** (1970) 1821.
[23] G. N. Dobrokhtov, *J. Appl. Chem. USSR*, **32** (1959) 2524.